Powder Technology 378 (2021) 455–467

Contents lists available at ScienceDirect

Powder Technology

journal homepage: www.elsevier.com/locate/powtec

Interplays between particle shape and particle breakage in confined continuous crushing of granular media

Fan Zhu *, Jidong Zhao

Department of Civil and Environmental Engineering, The Hong Kong University of Science and Technology, Clearwater Bay, Kowloon, Hong Kong SAR, China

ARTICLE INFO

Article history:
Received 28 July 2020
Received in revised form 23 September 2020
Accepted 5 October 2020
Available online 08 October 2020

Keywords:
Granular media
Particle crushing
Particle shape
Micromechanics
Multiscale modeling

ABSTRACT

This paper presents a computational study on the interactive evolution of particle shape and particle breakage for granular material under confined compression. A novel multiscale approach combining peridynamics and non-smooth contact dynamics is employed. Breakage of more than 12,700 particles with different size, shape, and loading condition are simulated with results examined statistically. It is found that, with the progress of particle breakage, the shape of fragments tends to achieve a steady state distribution. Particle shape has profound influence on the strength and crushing pattern of individual particles and such influence is best reflected by sphericity. The average particle strength appears linearly correlated with particle shape factors and sphere-like particles tend to possess higher strength and break in a major-splitting mode. The findings help to decode the intricate crushing behavior in granular media and shed lights on future development of physically informed, simplified models for predicting particle breakage.

1. Introduction

Grain crushing dictates key properties and performance of granular media that are important to a wide range of engineering and industrial sectors, including civil and chemical engineering and mining, food and pharmaceutical industries. Compaction, comminution, and grinding of granular materials often chase for best energy efficiency, calling for better understanding, simulation, and prediction of those processes. Grain crushing is also of great interest to geophysical research since it is a key mechanism in geoscience with relevance to cataclastic flow, localized deformation in porous rocks, and accretionary wedges. The process of grain crushing in granular media is featured by accompanied evolutions of both grain size and shape. Take natural sands as an example. It has been well accepted that continuous particle crushing leads to particle size evolving towards a fractal, in other words self-similar, distribution [1,2]. The grain-scale strength is dependent of particle size as a result of statistical distribution of micro-defects in the bulk of grain [3]. The evolution of particle shape is less investigated despite of the significant role of particle shape in mechanical properties of granular media such as packing, compressibility, strength, and critical state behavior [4–6]. Direct measurements on particle shape evolution along continuous crushing process were made possible recently with the aid of non-invasive techniques such as X-ray computed tomography. For single particles undergone crushing, significant alteration of major shape factors including flatness, elongation, and sphericity was observed [7,8], and distribution of the shape factors was found to follow statistical laws. For granular samples, the crushing-induced particle shape evolution was found to be most obvious in terms of sphericity and convexity as reported by Fonseca et al. [9] for sand specimens under triaxial compression. Zhang et al. [10] examined the evolution of particle shape with respect to aspect ratio, sphericity, and convexity after a large-strain shear and reported formation of self-similar distributions of those shape factors. Vafaei et al. [11] measured quartz sand particles undergone a ring shear and reported particle shape alternation from semi-angular to quasi-square.

The evolution of particle shape driven by crushing is never a "one-way" process. Grains with different shapes resulted from fragmentation affect the subsequent crushing of these fragments. There has been ample evidence indicating significant influence of particle shape on the strength of individual particles [12]. Meanwhile, a particle may crush with a variety of patterns [13,14] where particle shape plays a pivotal role [15]. Karatza et al. [16] used X-ray tomography to study crushing of zeolite particles placed in a granular sample and found particle shape (sphericity) has apparent effect on crushability and crushing mode. Direct measurements of grain-scale loading conditions in a granular assembly remain difficult experimentally, which limits the capability of experimental work on quantifying particle shape effects on its strength. Nonetheless, Hurley et al. [17] utilized an X-ray diffraction method to measure inter-particle contacts and forces during the fragmentation process, which allows assessments of crushing condition of particles with various shapes. Microscopic studies on such shape effect remain limited and are often restricted to a few particle shapes or loading conditions, which may not be adequately representative for granular

* Corresponding author.
E-mail address: fzhuaa@connect.ust.hk (F. Zhu).

https://doi.org/10.1016/j.powtec.2020.10.020
0032-5910/

media. A statistical study on particle crushing characteristics due to the shape effect is necessary to incorporate the great variance in particle shapes and loading conditions experienced by individual particles.

In this paper, we present a computational study on particle shape evolution and its interplay with the crushing characteristics during continuous crushing of granular sand. We employ a recent hybrid peridynamics (PD) and non-smooth contact dynamics (NSCD) approach developed by the authors [18] for the study. As will be shown, the approach enables the simulation of continuous particle crushing process while respecting and preserving the natural main features of particle shape. Simulation results are validated with experimental data with respect to single particle crushing strength, normal compression line (NCL), particle size distribution (PSD). The modeled particle shape is also compared with experimental measurement where possible. The evolution of particle shape factors including flatness, elongation, aspect ratio, and sphericity is rigorously analyzed. We further examine the influence of shape on particle crushing characteristics including strength and crushing pattern. The study aims to offer insights into the complex micromechanical behaviors of particle crushing which is often difficult or even impossible to explore experimentally, and to facilitate future development of physically informed, continuum models for crushable granular materials.

2. Numerical modeling

2.1. Methodology

The hybrid PD and NSCD approach utilizes non-smooth contact dynamics for simulation of the granular system and peridynamics for analyzing crushing of individual particles. The numerical approach is briefly described in the following while interested readers are referred to [18] for more details. In the presented work we employ an in-house code for peridynamic computations and open-source code *Project Chrono* [19] for NSCD based discrete modeling. Geometrical computations involved in the computing scheme are aided by *Computational Geometry Algorithms Library* [20]. Part of the results is visualized by an open-source application *Paraview* (https://www.paraview.org).

Peridynamics is a non-local method specialized in modeling fracture related problems in continuum media. A continuum domain is modeled as discretised interactive material points in PD. In this study, we apply the *ordinary state-based peridynamics* theory [21] with a linear peridynamic solid material model and a critical stretch damage model [22]. The same approach was utilized in a previous work [23] for modeling crushing of single sand grains. The NSCD [24] is an alternative discrete modeling approach to the commonly adopted, penalty-based DEM. It is favoured in this study mainly in view of its good computational efficiency [25] and ease in handling irregular shape particles since it solves contacts with a complimentary approach which bypasses complex algorithms in computing penalty-based contact forces. In NSCD, a granular system consisting of multiple rigid bodies involving collision, contact and friction is described by differential variational inequality (DVI) and solved by iterative approach [26]. In the present study we adopt a Gauss-Seidel based method with successive over-relaxation as the iterative solver to calculate the inter-particle contact forces. Particle motion is modeled by the Newton's second law. The inter-particle contact forces are used as input to the peridynamic analysis for breakage of individual particles. More details of the NSCD approach, as well as validation studies, are available in a variety of literatures [27–30] where interested readers are referred to.

The coupling of PD and NSCD follows the scheme presented in Fig. 1 and the computational procedures can be summarized into three major stages:

Stage 1

At designated time, particles are screened for breakage analysis based on a maximum contact force criterion. More precisely, if the maximum contact force on a particle is greater than a pre-defined threshold, the particle is considered “likely to break” and a breakage analysis will be carried out on it. Such a screening criterion roots in earlier studies which indicated that onset of crushing of a particle is closely related to the maximum contact force on it [17,23,31]. In this study we set the

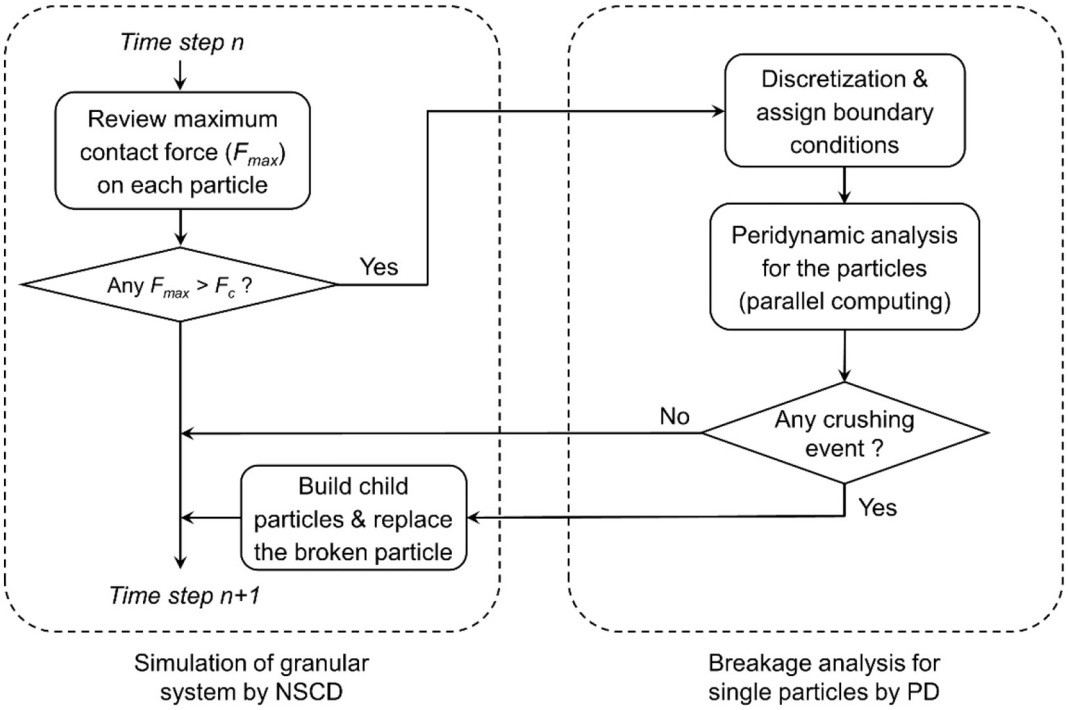

Fig. 1. Computational scheme of the hybrid PD and NSCD approach for grain crushing simulation.

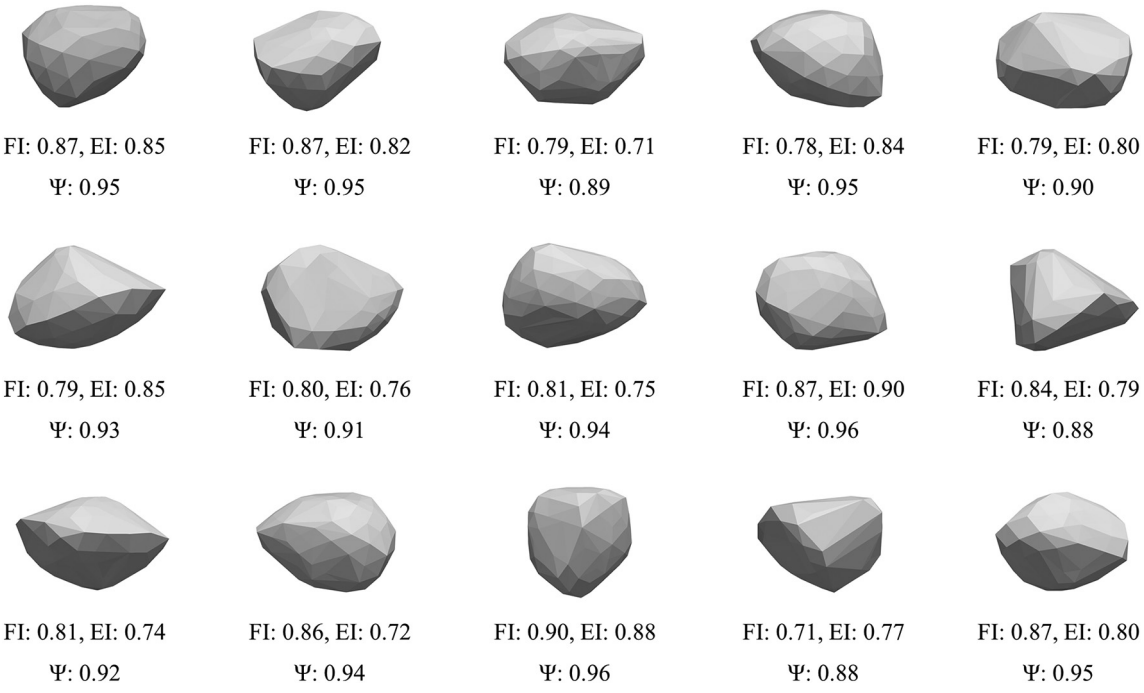

Fig. 2. The 15 particle shapes adopted for the sand packing in simulation. The single particle crushing strength is based on numerical testing for a particle with equivalent diameter of 1.7 mm and compressed between two parallel platens.

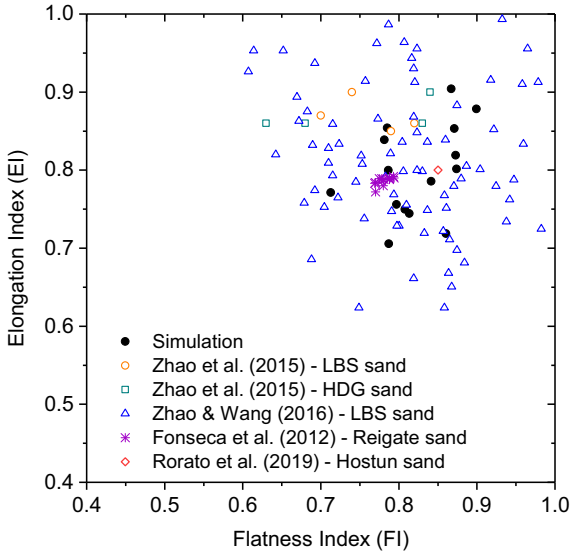

Fig. 3. Comparison of shape factors of modeled particle with typical sand particles in Zingg diagram.

breakage analysis threshold conservatively at about 80% of the uniaxial crushing force level of a particle.

Stage 2

For each particle selected in *Stage 1*, a peridynamic analysis is performed. The particle breakage analyses are made independent of each other and multi-thread parallel computing is implemented to speed up the computation. In each peridynamic analysis, the particle is discretized into material points following a cubic pattern with an element size of approximately 0.055*d* where *d* is the particle size, leading to about 3000 discretized points for each particle. Since the element size is selected proportional to the particle size, the same "resolution" will be applied in the peridynamic analysis for each particle. The inter-particle contact forces obtained in NSCD simulation are retrieved and modeled as boundary conditions in peridynamic analysis. Simplifications are made when applying those contact forces. In simple words, a prescribed contact zone is defined by a contact radius at each contact location. Material points within the contact zone are selected and contact force is applied on those points uniformly. Applying the contact force follows a constant rate until reaching the force magnitude as retrieved from NSCD simulation. The loading rate is carefully selected to avoid inertia effect. The above assumptions are simplifications to the real contact condition, which may be dependent of many

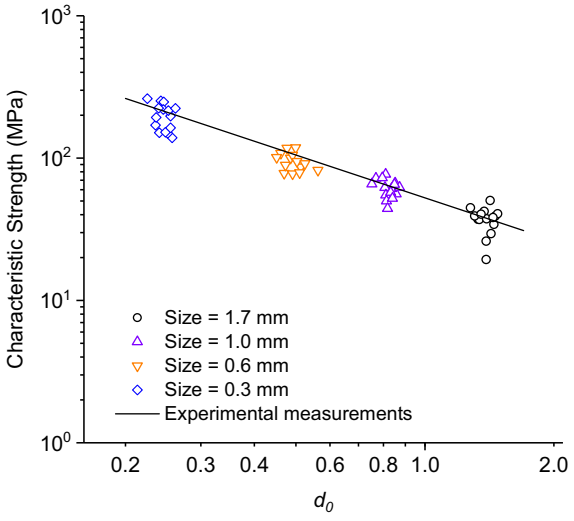

Fig. 4. Numerical tests of characteristic strength for single particles and comparison with experimental measurements by Nakata et al. [3]. To keep consistent definitions with the experiments, the symbol d_0 denotes the initial distance between the two parallel platens compressing the particle. The characteristic strength is calculated by dividing the maximum force before particle crushing applied by the square of d_0.

factors including the load, material and particle morphology. Further study may be carried out to model the contact conditions more precisely and investigate its effect on particle breakage. The technical procedures for applying the boundary conditions are described with more details in [18].

Stage 3

If any of the particles analyzed in *Stage 2* is found crushed, child particles will be built by either convex or concave polyhedrons. However, considering the high computational cost associated with contact detection involving concave shapes, we have modeled a particle as convex shape if it has convexity greater than 0.85 or an equivalent diameter smaller than 1.0 mm. Such simplification may reduce the accuracy of estimated shape factors of the fragments to some degree. Many fine fragments may form during fragmentation process which can also be reflected in peridynamic analysis. However, those fine fragments are not modeled for better computational efficiency although they also play a role in continuous particle crushing when they accumulate to a large amount. In discrete modeling, the crushed particles will be replaced with the child particles, occupying the same space. At the time immediately after crushing, the child particles may possess certain kinetic energy which is transferred from stored strain energy [32], such kinetic energy is not explicitly modeled in the view that it dissipates fast in a granulate system [33,34]. Time step is then advanced in discrete modeling and *Stage 1* is repeated at next designated time.

2.2. Sand particle modeling

2.2.1. Particle morphology

The shape of natural sand grains can generally be described on three scales [35]: *form*, *roundness*, and *surface texture* with a variety of shape factors on each scale. The *form* factors, such as ratios between the three dimensions of the particle, delineate the overall shape of a particle. Crushing of particles due to mechanical loadings is the major contributor to modification of the *form* factors. On smaller scales, *roundness* describes local surface features such as angularity at edges and corners [36,37] whereas *surface texture* represents the smallest scale features and is also referred to as roughness or smoothness. The most used *form* factors include elongation index (EI), flatness index (FI), and aspect ratio (AR). They are defined in the present study as I/L, S/I, and S/L, respectively, where S, I, L represent short, intermediate, and long dimension of a particle obtained from a box fitting approach [38]. A special shape factor refers to sphericity, which assesses deviation of a three-dimensional shape from perfect sphere. Sphericity is defined as the ratio between surface area of a spherical particle having the same volume and the surface area of the particle [36] and can be expressed by

$$\Psi = \left(\sqrt[3]{36\pi V_p^{\,2}}\right)/A_p \tag{1}$$

where V_p and A_p represent volume and surface area of the particle, respectively. The sphericity may be regarded as a *form* factor while admitting that it is influenced by both overall dimensions of a particle and local features at edges and corners [35].

In the present study we focus on modeling particle shapes and their evolution on the *form* scale. The three *form* factors mentioned earlier and sphericity are used to describe particle shapes. Investigation on other shape factors such as convexity, roundness, and roughness are beyond the scope of the current study since the particle morphology herein is not simulated to the scale that can satisfactorily describe those quantities. The shapes of sand grains for the simulated sample are generated using an open source code *Packing3D* following a Fourier descriptor approach [39,40]. All shapes are further simplified to convex polyhedrons as a balanced consideration between computational efficiency and simulation accuracy. Removing the local concavity features on particle surface results in higher sphericity but other shape factors remain preserved. Total 15 different particles are generated as exhibited in Fig. 2. The dimensional ratios of those particles are comparable to measurements for typical sand particles [7–9,41] as demonstrated in Fig. 3. The sphericities of the particles are mostly above 0.9 which is higher than average of what measured by Rorato et al. [41] and Zhao & Wang [8] but in line with the measurements by Fonseca et al. [9]. Those shapes are used later to form a granular sand sample for simulation (Fig. 5(a)).

2.2.2. Particle strength

Existing studies have shown that the strengths of natural sand particles follow Weibull distribution [3,42,43] and the survival probability of a particle can be described by:

$$P_s = exp\left[-\left(\frac{V}{V_0}\right)\left(\frac{\sigma}{\sigma_0}\right)^{\psi}\right] \tag{2}$$

where P_s denotes the survival probability of a particle with volume V under a characteristic stress of σ. σ_0 represents a characteristic strength at which 37% of the particles with volume V_0 survive. The characteristic strength is calculated by maximum applied force on a particle divided by the square of its size. Unless otherwise specified, the size of a particle in this paper refers to the diameter of a sphere having the same volume to the particle. The parameter ψ is Weibull modulus which typically ranges between 1 and 4 for sand [3,42–44]. For the sand studied herein, ψ is determined to be 3.0 based on single particle crushing experiments [3,13] and subsequent simulation results are compared with the same experimental work.

In numerical simulation, the strength of a particle is controlled in peridynamics by the critical energy release rate G_c. To implement the statistical strength distribution, proper G_c values have to be assigned to the particles in the initial packing. The Weibull distribution of particle strength can be implemented by

Table 1
Summary of parameters adopted in simulation.

Parameters	Value
Sand particle properties	
Density (kg/m^3)	2650
Young's modulus (GPa)	70
Poisson's ratio	0.17
Base critical energy release rate (J/m^2)	20
Restitution	0.0
Friction coefficient (inter-particle)	0.5
Friction coefficient (particle-boundary)	0.0
Weibull modulus	3.0
PD model	
Horizon [1]	$3\Delta x$
Loading rate (N/s) [2]	1.6×10^6
Contact zone radius (particle-platen) [3]	$2.5\Delta x$
Contact zone radius (inter-particle) [3]	$3.5\Delta x$
Influence function [4]	Gaussian
Discrete (NSCD) model	
Time step (s)	1×10^{-5}
Total simulation time (s)	0.8
Number of iterations each step	200

Notes: [1] Horizon is selected at 3 times element size as a typical practice in PD for modeling brittle fractures. [2] The loading rate is selected as a highest possible rate without generating inertia effect. Relevant numerical test is presented in [18]. [3] Particle-platen contact is modeled in single particle crushing test and inter-particle contact is modeled in compression of granular sample. Larger value is used for inter-particle contact in the view of smaller elastic modulus at contact comparing with particle-platen contact. [4] Gaussian influence function is used to reduce non-locality in the simulation. The Gaussian coefficient is taken to be 0.4.

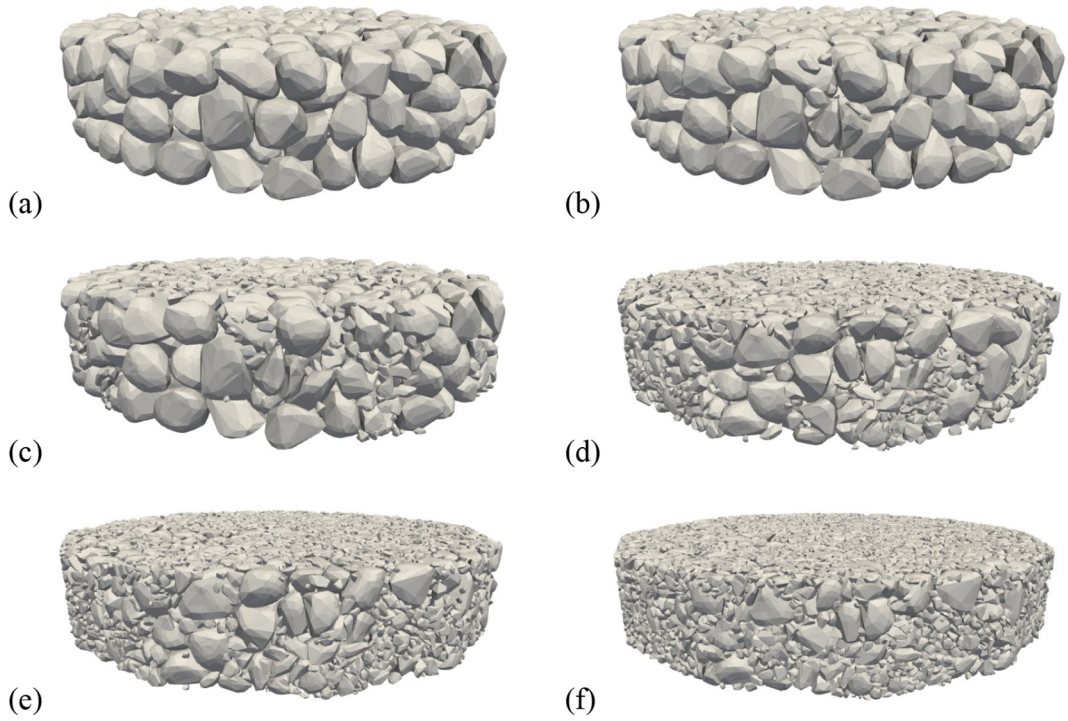

Fig. 5. Simulation of continuous crushing of sand sample under increasing loads: (a) initial state; (b) at 5 MPa; (c) at 10 MPa; (d) at 15 MPa; (e) at 20 MPa; (f) at 30 MPa.

$$\sigma_c = \sigma_{c0}[-\ln(U(0,1))]^{\frac{1}{\psi}}\left(\frac{V}{V_0}\right)^{-(1/\psi)} \tag{3}$$

where σ_{c0} is the characteristic strength of a reference particle and $U(0,1)$ is a random number drawn between 0 and 1. The reference particle is defined to have a characteristic strength corresponding to 37% survival probability. For spherical particles crushed under uniaxial forces, the critical energy release rate is correlated to particle strength by $\sigma \propto \sqrt{G_c}$ [18], so that the value of G_c for particles in the initial packing can be approximated by:

$$G_c = G_{c0}[-\ln(U(0,1))]^{\frac{2}{\psi}}\left(\frac{V}{V_0}\right)^{-(2/\psi)} \tag{4}$$

where G_{c0} represents critical energy release rate of a reference particle whose volume is V_0. The reference particle in the simulation is defined as a particle with a size of 1.7 mm and a characteristic strength of 30 MPa, according to the measurements by Nakata et al. [13].

The strength of sand particles shows apparent size effect as a result of heterogeneity in volumetric distribution of micro-defects. Smaller particles are found stronger than large ones [3,43]. Such effect is implemented in simulation when particle breakage occurs. The critical energy release rate of a child particle is determined by:

$$G_{ch} = G_{pr}\left(\frac{V_{ch}}{V_{pr}}\right)^{m} \tag{5}$$

where G_{ch} and G_{pr} represent the critical energy release rates for the child particle and parent particle, respectively. V_{ch} and V_{pr} refer to the volume of the child particle and parent particle, respectively. The factor m correlates the strength of a particle with its volume. To determine the value of m, we perform series of numerical simulations of single particle crushing for particles with different sizes, using the methodologies presented in Section 2.1. The 15 particles shown in Fig. 2 are all tested, with sizes at 1.7, 1.0, 0.6, and 0.3 mm. As demonstrated in Fig. 4, good agreement with experimental measurements is obtained with m taken as −0.35 and the value is adopted for subsequent simulation.

2.3. Simulation of 1-D compression

The simulated specimen consists of initially 523 particles placed in a rigid cylinder-like container with a radius of 22 mm and an initial height of approximately 5.1 mm. The modeled diameter-to-height ratio of the specimen is close to that in typical 1-D compression experiments [13,45]. The sand particles are nearly mono-disperse with sizes ranging from 1.5 to 1.7 mm. The shape of each particle is randomly assigned using the shapes presented in Fig. 2. The specimen is prepared by generating a "cloud" of particles followed by a deposition process under gravity. The initial void ratio of the sample is 0.635. Material properties

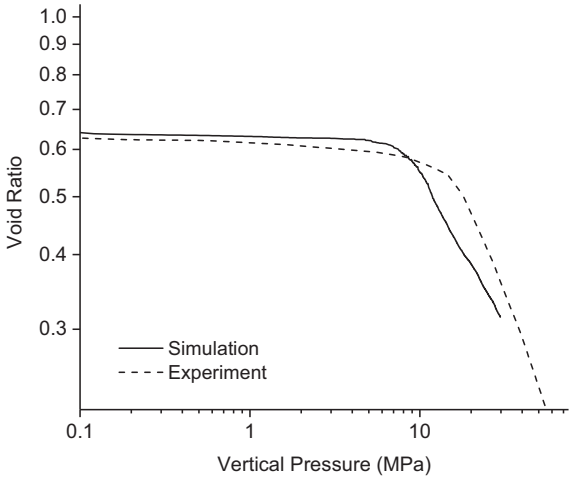

Fig. 6. The normal compression line and comparison with experiment.

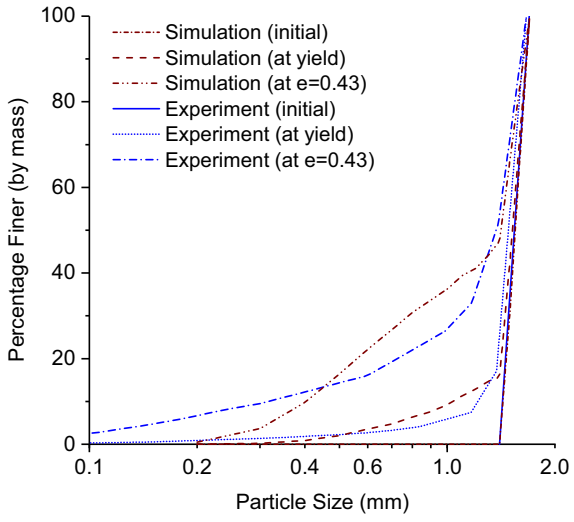

Fig. 7. Evolution of particle size distribution and comparison with experiment.

and other simulation parameters for the simulation are summarized in Table 1. The elastic parameters are selected in line with some past studies on sand [46,47]. A zero restitution is used as many experimental and numerical studies suggested that a multi-contact system can dissipate kinetic energies of shocks within very short time which leads to an effective restitution coefficient of zero [33,34]. The critical energy release rate of the reference particle is selected by calibration with measured single particle crushing strength and it is also within the tested range for quartz [48].

Vertical force is applied on a rigid platen modeled at the top of the specimen with load increasing at a constant rate until a maximum pressure of 30 MPa is reached. The total simulated time is 0.8 s with a time step size of 1×10^{-5} s. The loading rate, although appears high, does not incur inertia effect in the simulation. This is due to the nature of the complementarity approach in NSCD which assumes particles to be perfectly rigid and the incremental load spreads "instantly" in a dense contact network. Crushing of particles is analyzed at an interval of every 240 steps. This is based on a balanced consideration between simulation speed and accuracy. More frequent screening of particle crushing is expected to offer more realistic results since particle crushing can be identified promptly. Nonetheless, it may lead to excessive computational cost of the frequency is selected unnecessarily high. Sand is known to have a comminution limit beyond which crack propagation and brittle failure will not occur [49]. To reflect such physics, a crushing limit is set at 0.2 mm (although actual comminution limit is much smaller) and any particles with smaller size is assumed to be non-crushable.

The simulated specimen is visualized in Fig. 5 which shows sign of significant particle crushing due to compression. The NCL obtained from simulation is shown in Fig. 6 together with experimental records [13]. Both curves consist of three portions: an elastic compression part where the void ratio of the sample slightly decreases, a yielding point where the curvature exhibits apparent change, followed by a virgin compression line. There remain some differences between the simulation and experiment. Notably, the yield stress as indicated by the point of maximum curvature is about 8 MPa in the simulation and is lower than experimental observation of about 14 MPa. In other words, the sample is weaker in simulation than the actual condition. The difference could possibly be attributed to the interlocking between irregular shape particles and the abrasion and breakage of small asperities [13], both phenomena may result in larger inter-particle contact area and higher strength against crushing but are not fully quantified in the numerical model. The virgin compression line reflects plastic deformation due to continuous crushing of particles. The PSD evolves with the progress of virgin compression. The PSD curves at the initial state, yielding point, and near end of the compression is plotted in Fig. 7. Overall agreement can be observed while admitting that fine fragments are modeled to a limited amount in the simulation due to the set crushing limit. Besides, the simulation focuses on modeling bulk crushing of particles so that the asperity breakage events may not be extensively modeled, hence the amount of particles in the 0.5 mm to 1.1 mm range tends to be more than actual measurement while the fine fragments tends to be less.

Another important attribute of particle crushing, which will be further discussed later, is the modification of particle shape. The experiment used for validation with respect to compressional behavior and particle size evolution does not offer measurement of particle shapes. Nonetheless, available evidences in literatures show that the shape of sand particle fragments is more elongated and angular than the state before crushing in both single particle crushing test [7,8] and compression of granular sample [50]. The effect is reflected by decreasing of dimensional ratios and sphericity with particle size. In our simulation, the same effect is observed as illustrated in Fig. 8. The particles in the initial packing, with sizes ranging from 1.5 to 1.7 mm, have average sphericity of about 0.93 and aspect ratio near 0.67. After a substantial crushing process, the small fragments (e.g., with sizes below 0.5 mm) are found to have average sphericity below 0.85 and aspect ratio below 0.55. The trend is consistent with the observation in experiment by Altuhafi & Coop [50] and good quantitative agreement is noted with respect to sphericity. The aspect ratio for small particles in the simulation appears lower than what measured. This could be possibly due to the attrition and breakage of asperities that were not fully accounted in simulation.

The above examinations confirm the reasonableness of the simulation results from various aspects. On single particle level, the particle strengths and shapes are modeled according to experimental measurements on sand particles. For the granular sand undergone 1-D compression, the simulation results are comparable to experimental records with respect to particle size distribution, normal compression and particle size-shape relations. The simulation records more than 12,700 particle crushing events, which offers a database for statistical examination on the interplays between particle shape and crushing. In the following sections, we extend our study to examine particle shape

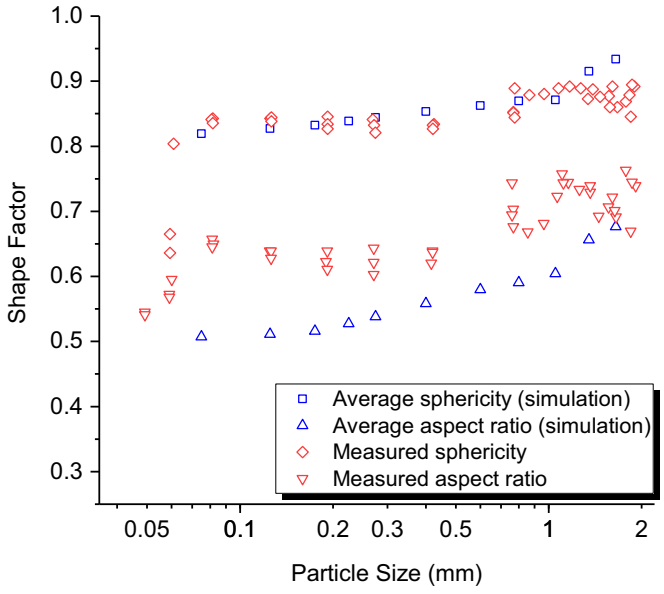

Fig. 8. Relation between particle size and particle shape factors. Simulation data is extracted at loading level of 30 MPa and is compared with experiment by Altuhafi & Coop [50].

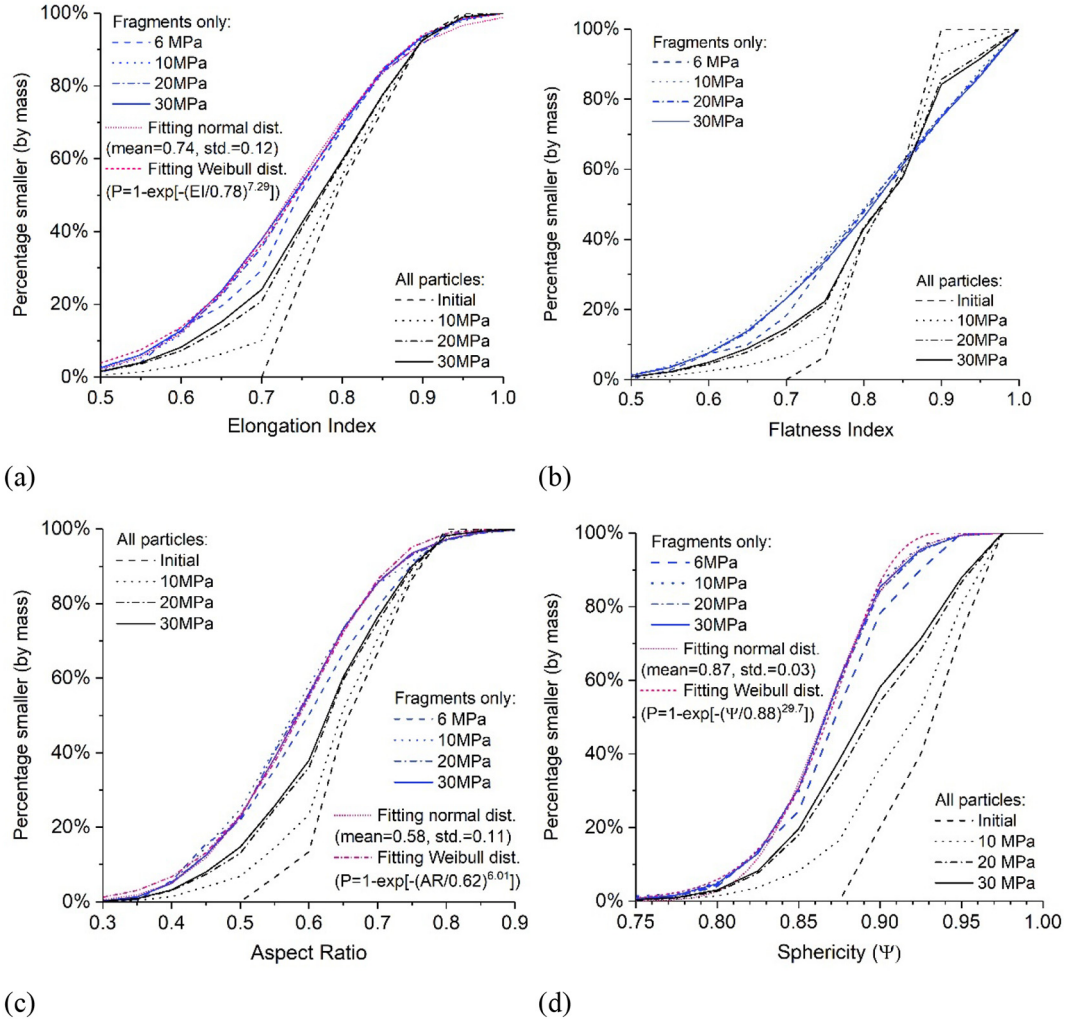

Fig. 9. Evolution of shape factors of the fragmented particles during continuous crushing process: (a) EI; (b) FI; (c) AR; (d) sphericity.

evolution during fragmentation and its interaction with the crushing characteristics.

3. Crushing induced particle shape evolution

The evolution of particle shape with the progress of particle crushing is examined statistically. Cumulative distribution of the dimensional ratios and sphericity of particles at different stress levels are presented in Fig. 9. The horizontal axis indicates value of the shape factors and the vertical axis presents percentage of particles (by mass) having smaller shape factors. Two sets of plots are presented concurrently, one considers the fragmented particles only (i.e., the particles in the initial packing are excluded) and the other accounts for all particles. The first set of plots may better reflect the effect of crushing on particle shape while the latter set shows the rate of shape evolution for the specific sample. Two major observations can be made. *First*, for the plots that considers fragments only, the distributions of the shape factors evolve quickly with increasing load and tend to approach steady state profiles. No apparent difference is seen for the shape distribution shortly after the yielding point, i.e., 10 MPa. The obtained steady-state profiles may be regarded as an intrinsic feature of granular materials undergone fragmentation. For the full sample, the shape distributions appear to evolve towards such steady-state profiles with decreasing rates. Observably, the

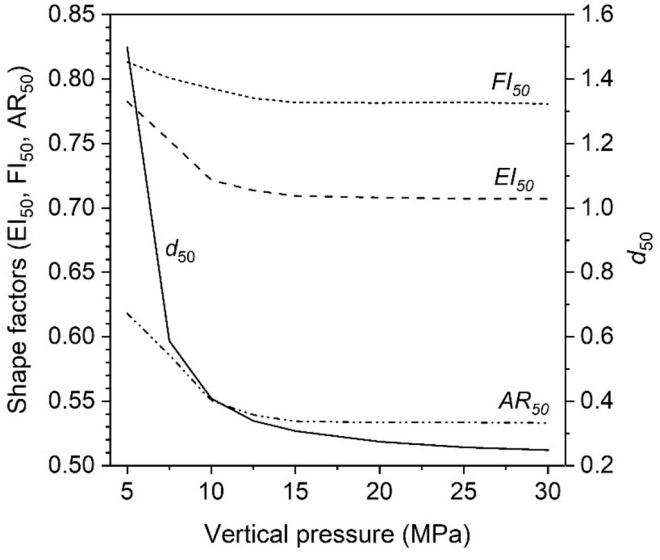

Fig. 10. The evolution of median particle size (d_{50}) and median shape factors (EI_{50}, FI_{50}, AR_{50}) with particle crushing.

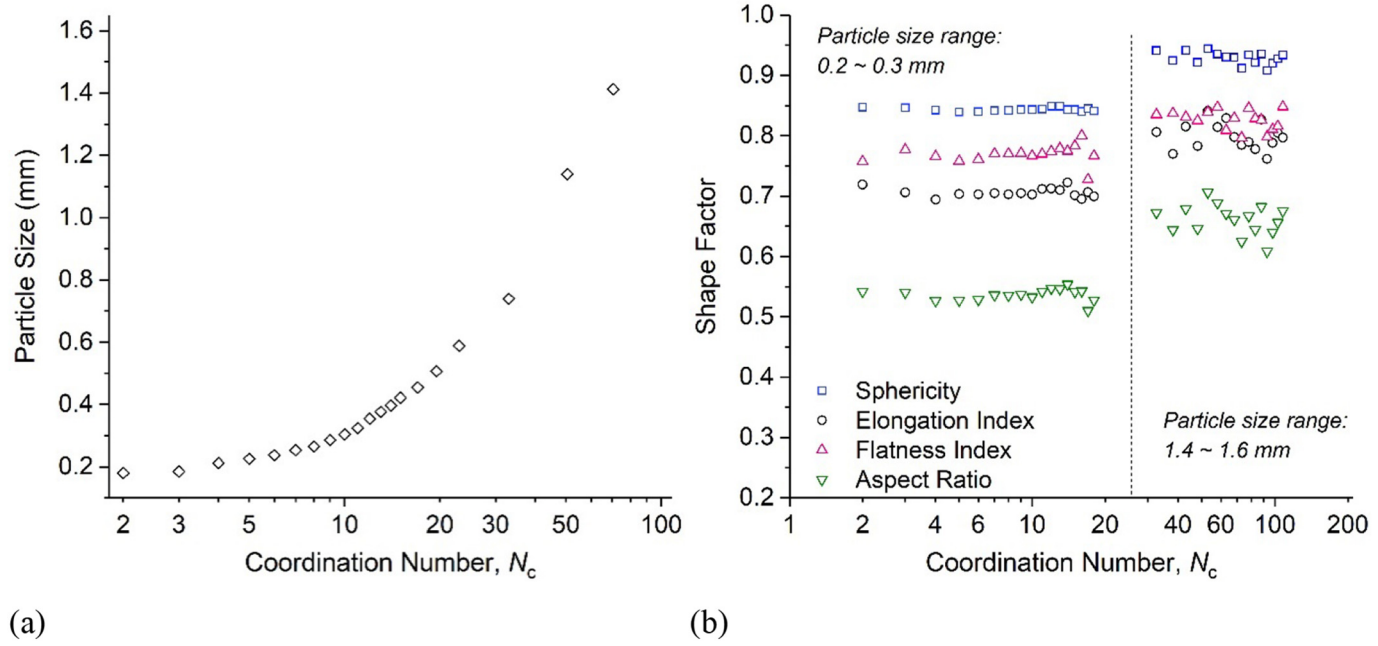

Fig. 11. The relation between coordination number, particle size, and particle shape: (a) average particle size versus coordination number; (b) average particle shape versus coordination number for particles with size range 0.2– 0.3 mm and 1.4– 1.6 mm. The data is extracted at the end of the simulation.

evolution of particle shape is much slower beyond 20 MPa than that before 20 MPa. It can however be expected that the shape distributions of the full sample will eventually approach the steady-state profiles (as implied by the fragments) if particles continue to crush under increasing load. *Second*, the distributions of all shape factors have an approximate lower limit. For EI and FI, the distributions start at about 0.5, indicating particles having EI or FI less than 0.5 are rare. Indeed, highly elongated or flat particles are uncommon in a continuous crushing circumstance since they can easily be buckled and are prone to breakage. The distribution of AR and sphericity start at about 0.3 and 0.75, respectively.

No consensus has yet been reached as to what statistical model can best describe the steady state shape factor distribution resulted from continuous grain crushing. Both normal distribution [35,51] and Weibull distribution [8] have been reported in the literature. We have attempted to describe the distribution of shape factors for the fragments with our obtained results by both models as shown in Fig. 9. Our examination suggests that both statistical models can describe the distribution of EI, AR, and sphericity to a reasonable extent, although normal distribution appears to perform better. The key parameters of cumulative distribution function suggested for the two statistical models are also shown in the figure.

It is important to realize the evolution of particle shape occurs with the reduction of particle size. To better illustrate the relationship between particle shape evolution and size evolution, the median values of particle size (d_{50}) as well as the median values of EI, FI, and AR of particles in the sample, denoted as EI_{50}, FI_{50}, and AR_{50}, respectively, are plotted in Fig. 10. The median size, as expected, decreases with continuous particle crushing. Such size reduction slows down at high stress range. The median values of EI, FI and AR decrease most quickly with the onset of particle crushing which is before the yielding of the sample. They continue to decrease at a lower rate after yielding, and appear to approach steady levels soon after yielding, to values near 0.71, 0.78 and 0.53, respectively. It is also noted that similar observations, which indicate convergence of shape factor distribution towards a steady state, was reported in some previous studies with different approaches [52,53].

4. Shape effect on particle crushing

4.1. Crushing strength

In this section, we assess particle shape effect on particle strength based on the data obtained from the model which contains more than 12,700 crushing events for particles with various shapes and loading conditions. To examine the shape effect on particle strength, it is important to exclude other effects as far as possible to avoid disturbance to the

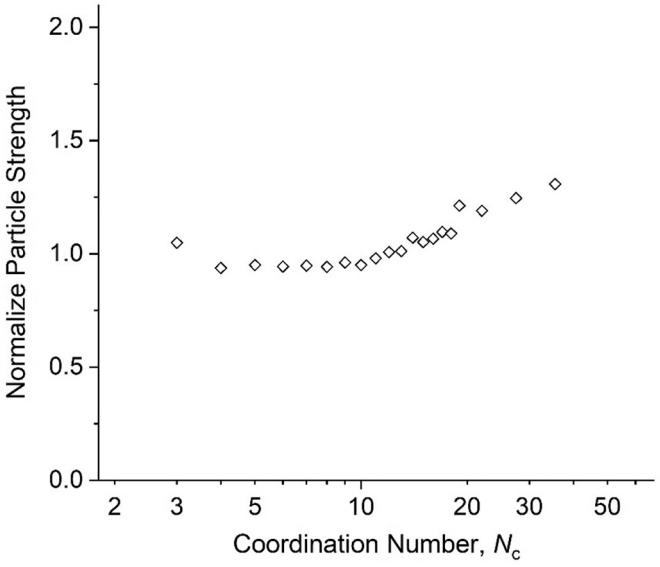

Fig. 12. The influence of coordination number on particle strength. The particle strength refers to the average strength of all particles having the coordination number. The plot covers all particle crushing data collected from the simulation up to a vertical stress level of 30 MPa.

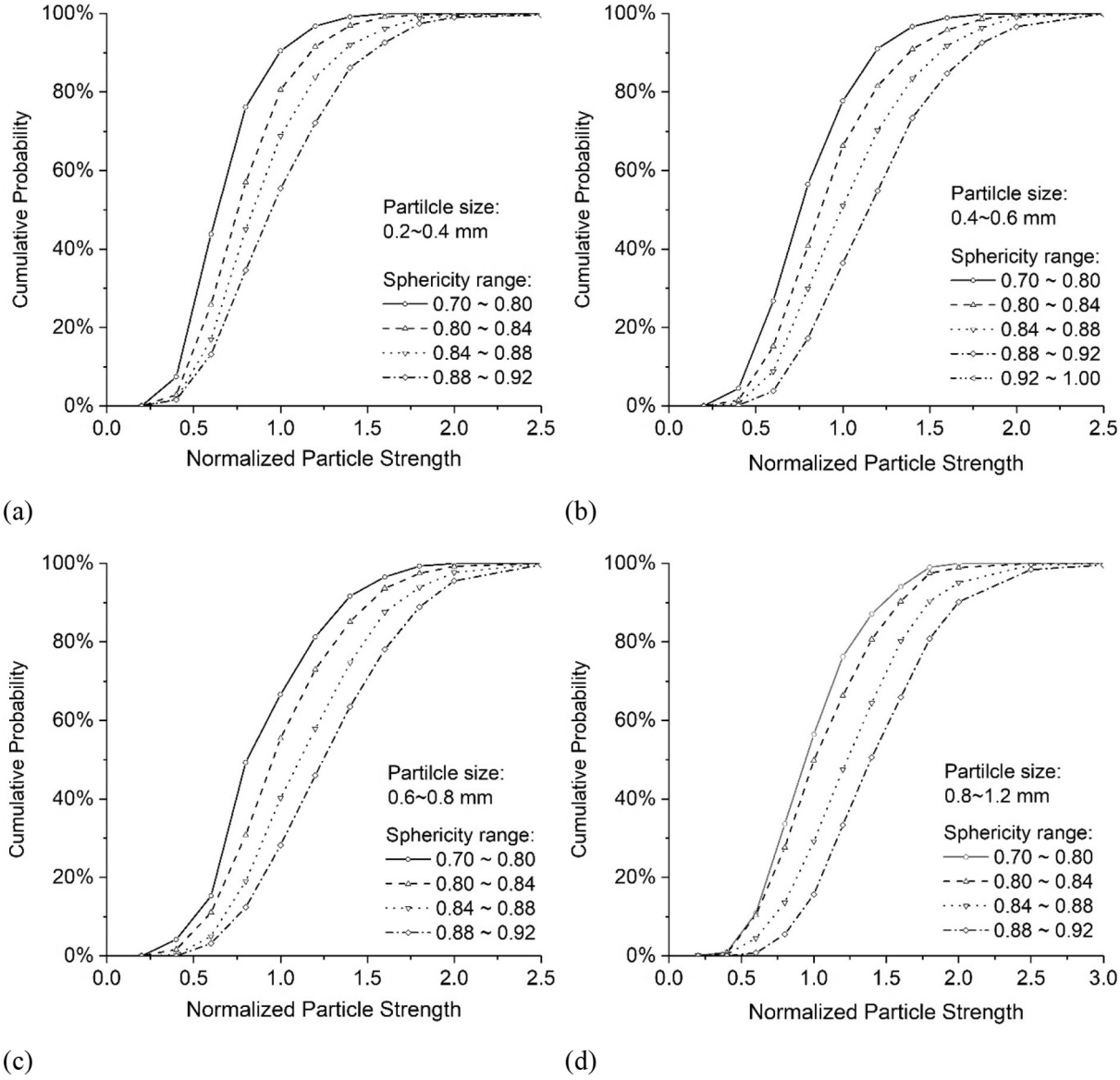

Fig. 13. Effect of sphericity on particle strength for different particle size categories: (a) 0.2 to 0.4 mm; (b) 0.4 to 0.6 mm; (c) 0.6 to 0.8 mm; (d) 0.8 to 1.2 mm. Some lines are not smooth due to limited data in that size or shape range.

observation. The major microscopic factors (other than shape) that affect particle strength include: i) particle size effect which originates from volumetric distribution of micro-defects, resulting in small particles being stronger than large ones; ii) variation of particle strength following Weibull distribution as observed from experiments; and iii) the loading condition experienced by particles in granular media during the loading process. The former two effects are implemented in the simulation as described in Section 2.2.2. The latter effect is expected to be more pronounced with the progress of particle crushing which drives the particle size distribution towards a highly polydispersed state. At that state, the large particles may be surrounded by numerous small particles which form a "cushion". High coordination number (N_c) can be expected for those large particles and that may influence the strength of particles [15,54]. In this study, the former two effects are explicitly removed via a normalization process to the particle strength obtained from simulation and the latter effect is avoided by assigning particles into different size groups when reviewing the results. The normalization to particle strength can be expressed by

$$\sigma_{nc} = \frac{\sigma_c}{\sigma_r} \tag{6}$$

where σ_c denotes the strength of a particle with size d and critical energy release rate of G_c. The strength of a particle herein refers to the characteristic strength calculated by the maximum normal contact force on the particle divided by square of particle size. Such definition originates from the common expression of characteristic strength [55]. The denominator σ_r is a theoretical strength of the particle if it crushes under uniaxial loading. σ_r can be derived in two steps. First, a base case is set with a reference particle having size $d_0 = 1.7$ mm crushed under uniaxial loading. The reference particle has a critical energy release rate as listed in Table 1. Note the definition of particle strength in this study (which uses equivalent diameter as particle size) is different from that typically used in single particle crushing test (where particle size refers to the distance between loading platens) because the platen distance concept is no longer applicable in multi-directional loading scenario. The particle strength in the base case is found to be $\sigma_0 = 20$ MPa. Second, the uniaxial crushing strength of the particle with size d is derived

from σ_0 and based on the relation of $\sigma \propto d^{-3/\psi}$. The variation in critical energy release rate (which was introduced in the initial packing) is considered by employing Eq. (5) and the relationship of $\sigma_c \propto \sqrt{G_c}$ [18]. Finally, the normalizer, σ_r, can be calculated by

$$\sigma_r = \sigma_0 \left(\frac{d}{d_0}\right)^{-(3/\psi)} \left[\frac{G_c}{G_0}\left(\frac{d}{d_0}\right)^{-3m}\right]^{1/2} \tag{7}$$

The value represents a theoretical strength, as derived from the base case, for a particle with size d and critical energy release rate G_c if it crushes under uniaxial loading. The normalized strength, σ_{nc}, therefore reflects how the strength of a particle, with its own size and shape and crushed under multi-directional loading, compares with the uniaxial crushing strength which is measurable in experiment.

As mentioned earlier, the loading condition experienced by a particle may affect particle strength. Here we use N_c as an indicator of the loading condition experienced by a particle. It should be realized that N_c is not an independent factor but is potentially related to particle size and shape. The relationship between particle size and N_c at end of the simulation (i.e., loading level of 30 MPa) is examined as shown in Fig. 11(a). It is clear that, after a substantial crushing process, the large particles have significantly more contacts than those small ones, since they are surrounded by numerous small fragmented pieces. On the other hand, the shape of particles does not seem to have a strong correlation with N_c. This is illustrated in Fig. 11(b) for particles in both small and large size ranges. For small particles, as they may be sheltered by the large ones, their shape does not play an important role on the number of contacts. For large particles, as they are surrounded by fragments, there is always a large number of contacts no matter they are elongated/flat or sphere-like. Theoretically it may be expected that large particles with lower sphericity have more contacting neighbours as they have a larger exposed surface area. Such shape effect appears to be insignificant within the investigated range and is believed to be much weaker than the effect of particle size. Finally, the effect of N_c on particle strength is examined as illustrated in Fig. 12. A general finding is that

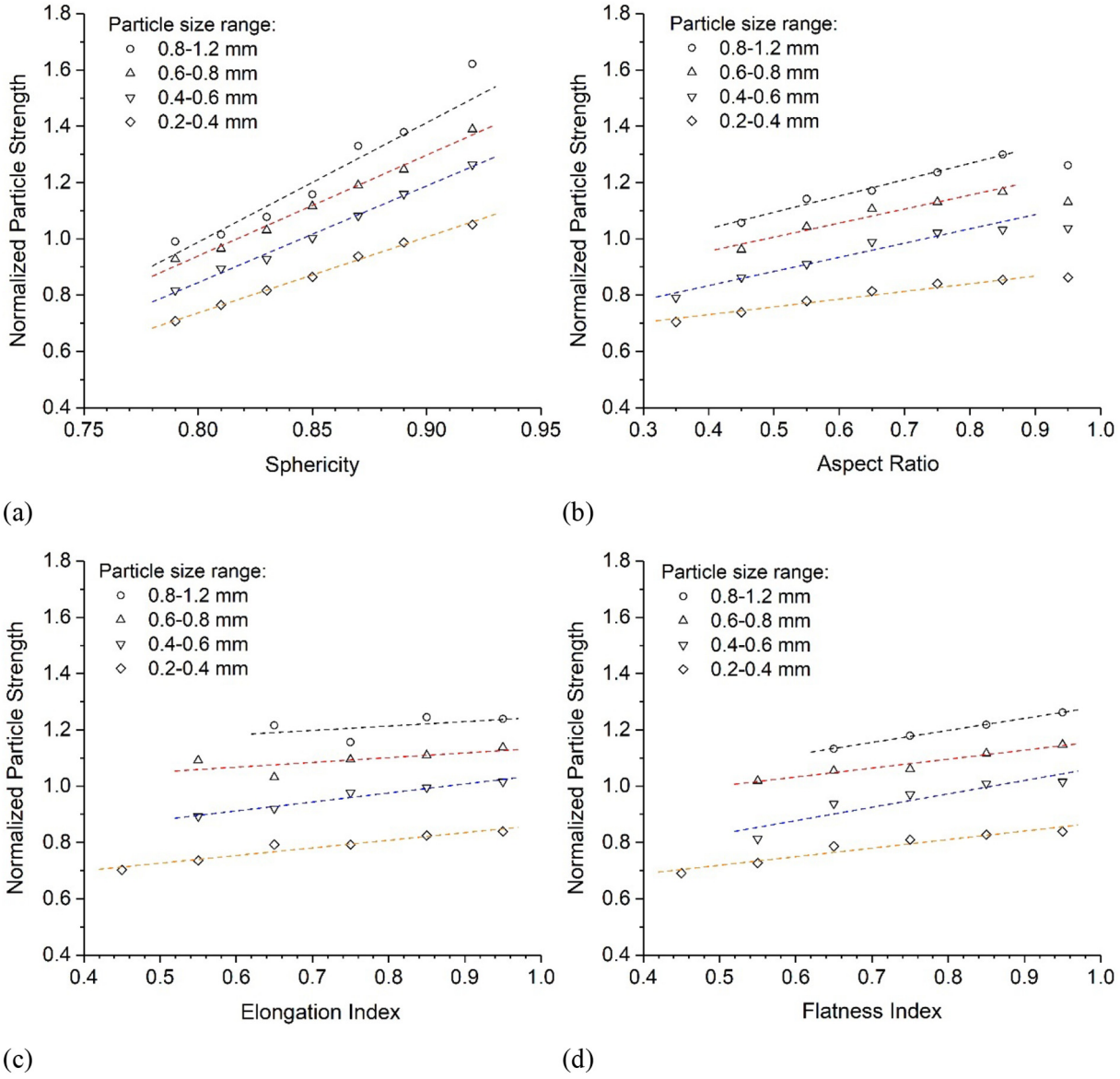

Fig. 14. Effect of particle shape on strength: (a) effect of sphericity; (b) effect of AR; (c) effect of EI; (d) effect of FI. The particle strength is an average strength of all particles with the specified size and shape. In (a) each plotting point includes data with sphericity ±0.1. In (b) to (d) each plotting point includes data with shape factor ± 0.5. A linear trend line for each set of data is shown for reference.

when the N_c is below 10, the average particle strength does not vary apparently. This is in line with previous finding that the particle strength does not bear a strong correlation with N_c when N_c is below 8 [23]. For particles with N_c above 10, its strength shows an increasing trend with N_c. Such effect should be mainly attributed to dispersion in particle size rather than particle shape.

To examine the shape effect on particle strength while avoiding the influence of coordination number, we divided particles into several size groups and particles in each group are expected to have similar N_c. With that, the relation between particle strength and sphericity is first reviewed and shown in Fig. 13. It indicates that, for particles in all size ranges, higher sphericity leads to higher strength. It may be expected that similar relation exists for other shape factors, since higher sphericity in general corresponds to higher dimensional ratios. Due to the limited space the plots for other shape factors are not included. To offer a more direct observation of the shape-strength relation, the average particle strength is plotted against the four shape factors as shown in Fig. 14. It confirms that higher values of sphericity, AR, EI, and FI generally lead to higher strength of particles against crushing. For instance, a particle having sphericity below 0.8 may be expected to have a strength of only 70% of that for a particle with sphericity above 0.9. The shape-strength relationship appears to be linear. The factor of sphericity seems to be better in describing the shape-strength relation in the view that the curve is monotonic with minimum fluctuation for all size ranges. For the other shape factors of AR, EI and FI, the shape-strength relationship follows the same trend, but the variation is at a smaller magnitude. The fluctuations in some curves are probably due to limited data in that size or shape range. The good performance of sphericity in describing the shape effect indicates that particle strength is likely related to local features of particles, such as angularity at edges and corners, since they are accounted for (at least partially) by sphericity. The findings also suggest that a liner term may be added into Eq. (2) to account for the effect of particle shape.

4.2. Crushing patterns

Crushing pattern of single particles is quantitatively examined in this section based on characteristics of the fragments. More specifically, the study is carried out from two aspects: i) the particle shape effect on the mode of breakage; and ii) particle shape effect on the shape of fragments. Modes of breakage were classified by Nakata et al. [13] into five types, covering a wide range of status from no visible damage to asperity breakage and major splitting. In this paper our main interest lies on asperity breakage and major splitting type of breakage. Relevant size of the fragments is an important indicator for differentiation between the two types of breakage. The asperity breakage is defined here as a crushing event where the largest fragment has a volume not less than 70% of the parent particle. Such definition is analogous to that by Nakata et al. [13] which uses 70% cross-sectional area as a threshold to differentiate the two types of breakage. If none of the fragments have volume on or above such threshold, the crushing is considered as a major splitting type. Percentage of occurrence of the two types of breakage with respect to parent particle shape is examined in Fig. 15. It is generally observable that increasing sphericity leads to an increasing probability of breakage under major splitting mode. For particles with sphericity higher than 0.9, about 80% crushing events are of major splitting type, rising from 60% when the particle possesses lower sphericity. Similar trend is however not apparent with respect to dimensional ratios such as AR (Fig. 15(b)). It is noted the results also coincide with the observation by Nakata et al. [13], which does not differentiate the particle shape and suggests that 60% of the particles undergone breakage fit the criterion of major splitting.

The influence of particle shape on the shape of its immediate fragments is examined with respect to sphericity and AR as shown in Fig. 16. For a particle with any given shape, the shape of its immediate fragments has a wide possible range. The probability distribution for the shape of the fragments is indeed related to the shape of parent particle. For parent particles possessing small sphericity (e.g., those with elongated, flattened, and/or angular shapes), their immediate fragments also tend to have relatively small sphericity and vice versa. Such phenomenon can be explained by the good chance of asperity breakage for those elongated or flattened particles as reflected in Fig. 15. In such mode of breakage, the main body of the parent particle is largely preserved so that its geometrical feature remains similar to the status before breakage, although the loss of asperities may lead to gain in sphericity. Another possible explanation is that for sphere-like particles, the higher strength allows accumulation of higher strain energy inside the particle before breakage, which facilitates branching

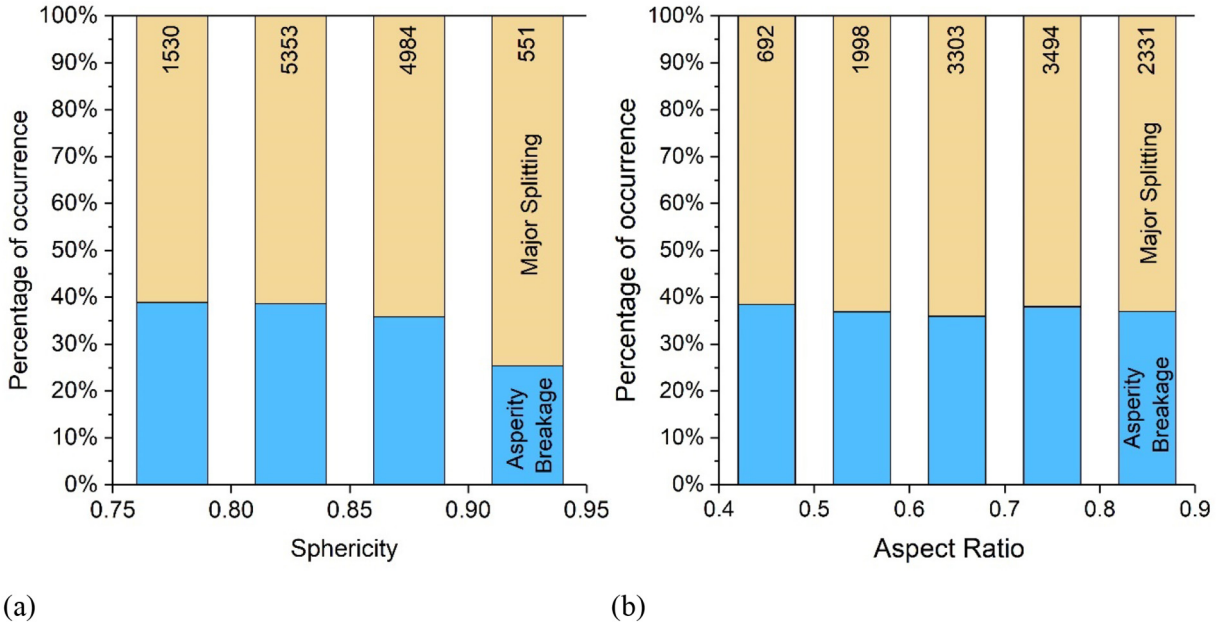

Fig. 15. Particle shape effect on breakage mode: (a) influence of sphericity; (b) influence of AR. The number at top of each bin indicates the total number of crushing events recorded.

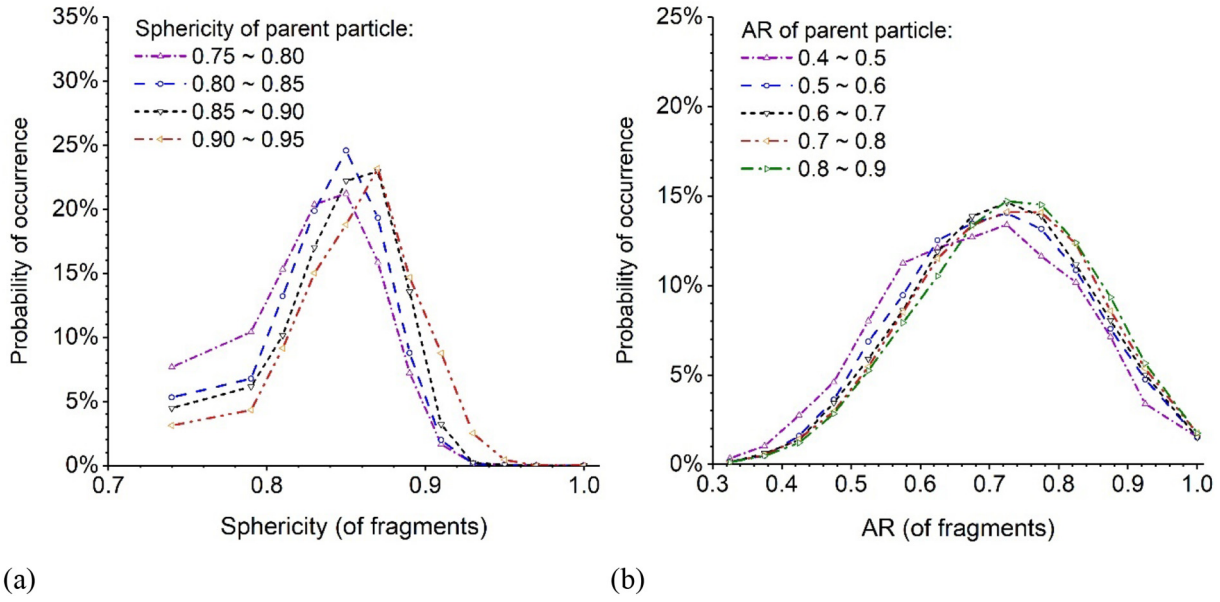

Fig. 16. Probability distribution of shape factors in single particle crushing events: (a) sphericity; (b) AR.

and jointing of cracks between the multiple contact points on the particle and may reduce the likelihood of formation of highly elongated or flattened fragments. Similar shape effect can also be observed with respect to AR although the variation seems mild. It can be pointed out based on the observation that local morphology of particles plays an important role in the shape of the fragments. Sphericity appears to be better than other form factors in describing particle shape effect on the shape of fragments, in the view that it accounts for local features of particles to some degree. It can be further commented that factors such as angularity or roundness may also reflect such shape effect, though detailed investigation on those factors is beyond the scope of this study.

5. Conclusions and outlook

We numerically examined the interplays between particle shape evolution and continuous crushing of particles in granular media. The study delineates a picture on particle crushing where particle shape plays an important role together with particle size and microscopic loading conditions. Conclusions are made on the following aspects of the complex process of crushing in granular media:

1. Continuous crushing of particles drives steady evolution of key particle shape factors including EI, FI, AR and sphericity. With progress of crushing, the distribution of each of the shape factors for the fragments approaches a steady profile which may be approximated by a normal or Weibull distribution. The progress of fragmentation is accompanied by a gradual reduction in the median size of fragments while median values of EI, FI and AR of the fragments evolve to steady values soon after yielding.
2. Particle strength is affected by a variety of factors including particle size, statistical variation of particle strength, loading conditions, and particle shape. The loading conditions of a particle, as indicated by coordination number, is found to influence particle strength and such effect is mainly linked with particle size. To review particle shape effect on particle strength, other effects are filtered out by normalization to particle strength and categorizing particles into different size groups. Particle shape is found to have apparent influence on strength. Sphericity is considered best in describing the shape-strength correlation while the dimensional ratios including AR, EI and FI reveal similar trend. Particles with higher sphericity possess higher strength on average. The shape effect can be approximated by a linear relation between shape factors and particle strength.
3. Shape also affects the crushing pattern of particles in terms of breakage mode. It is found that sphere-like particles are likely to undergo a major-splitting type of breakage with about 80% recorded cases being major-splitting. The shape of fragments produced in single particle crushing event is also found relevant to the shape of parent particles. Particles with smaller sphericity generally result in fragments also having smaller sphericity and vice versa. The shape effect on crushing pattern is best captured by the factor of sphericity. The findings suggest that particle crushing characteristics are related to both overall dimension of a particle and local morphologies.

The presented work has demonstrated the complexity of interplay between evolving particle shape and particle breakage during continuous crushing of granular materials which demands proper computational tools such as the one presented to render a quantitative examination with physical insights. While the study has focused on microscopic characteristics of particles, linkage of the observations to macromechanical behaviors of granular media is necessary yet challenging in future. In particular, the quantitative observations made in this study, if further aggregated and confirmed with further data of more complex loading cases, can be made useful for extension of continuum breakage mechanics [56] to incorporate information on particle shape and energy consumption during continuous crushing process of a granular material. Understandably, the breakage and morphology change of real natural granular materials can be tremendously complex. A great variety of factors may potentially affect particle breakage and shape evolution, including but not limit to contact conditions between particles [15], mode of loading [50], ambient environment [57], and inhomogeneity and anisotropy of materials [58]. Detailed examinations on those factors in correlation with particle shape would be interesting for future extension of the current work.

Declaration of Competing Interest

The authors declare that they have no known competing financial interests or personal relationships that could have appeared to influence the work reported in this paper.

Acknowledgments

The study was financially supported by the National Natural Science Foundation of China under project 11972030 and Research Grants Council of Hong Kong through GRF Project 16205418, CRF Project C6012-15G and TBRS Project T22-603/15-N. The first author acknowledges financial support from Hong Kong Ph.D. Fellowship Scheme funded by Research Grants Council of Hong Kong.

References

[1] D.L. Turcotte, Fractals and fragmentation, J. Geophys. Res. 91 (B2) (1986) 1921–1926.
[2] G.R. McDowell, M.D. Bolton, On the micromechanics of crushable aggregates, Géotechnique 48 (5) (1998) 667–679.
[3] Y. Nakata, Y. Kato, M. Hyodo, A.F.L. Hyde, H. Murata, One-dimensional compression behavior of uniformly graded sand related to single particle crushing strength, Soil Found. 41 (2) (2001) 39–51.
[4] G.C. Cho, J. Dodds, J.C. Santamarina, Particle shape effects on packing density, stiffness, and strength: natural and crushed sands, J. Geotech. Geoenviron. 132 (5) (2006) 591–602.
[5] J. Mellmann, T. Hoffmann, C. Fürll, Flow properties of crushed grains as a function of the particle shape, Powder Technol. 249 (2013) 269–273.
[6] S. Zhao, N. Zhang, X. Zhou, L. Zhang, Particle shape effects on fabric of granular random packing, Powder Technol. 310 (2017) 175–186.
[7] B. Zhao, J. Wang, M.R. Coop, G. Viggian, M. Jiang, An investigation of single sand particle fracture using X-ray micro-tomography, Géotechnique 65 (8) (2015) 625–641.
[8] B. Zhao, J. Wang, 3D quantitative shape analysis on form, roundness, and compactness with μCT, Powder Technol. 291 (2016) 262–275.
[9] J. Fonseca, C. O'Sullivan, M.R. Coop, P.D. Lee, Non-invasive characterization of particle morphology of natural sands, Soils Found. 52 (4) (2012) 712–722.
[10] X. Zhang, W. Hu, G. Scaring, B.A. Baudet, W. Han, Particle shape factors and fractal dimension after large shear strains in carbonate sand, Géotech. Lett. 8 (1) (2018) 73–79.
[11] N. Vafaei, K. Fakharian, A. Sadrekarimi, An experimental study on effect of boundary condition on particle damage in shear zone of crushed sand, J. Geophys. Res. 124 (2019) 9546–9561.
[12] R. Fu, X. Hu, B. Zhou, Discrete element modeling of crushable sands considering realistic particle shape effect, Comput. Geotech. 91 (2017) 179–191.
[13] Y. Nakata, M. Hyodo, A.F.L. Hyde, Y. Kato, H. Murata, Microscopic particle crushing of sand subjected to high pressure one-dimensional compression, Soils Found. 41 (1) (2001) 69–82.
[14] W. Wang, M.R. Coop, An investigation of breakage behaviour of single sand particles using a high-speed microscope camera, Géotechnique 66 (12) (2016) 984–998.
[15] M.C. Todisco, W. Wang, M.R. Coop, K. Senetakis, Multiple contact compression tests on sand particles, Soils Found. 57 (1) (2017) 126–140.
[16] Z. Karatza, E. Ando, S.A. Papanicolopulos, G. Viggiani, J.Y. Ooi, Effect of particle morphology and contacts on particle breakage in a granular assembly studied using X-ray tomography, Granul. Matter 21 (2019) 44.
[17] R.C. Hurley, J. Lind, D.C. Pagan, M.C. Akin, E.B. Herbold, In situ grain fracture mechanics during uniaxial compaction of granular solids, J. Mech. Phys. Solids 112 (2018) 273–290.
[18] F. Zhu, J. Zhao, Modeling continuous grain crushing in granular media: a hybrid peridynamics and physics engine approach, Comput. Methods Appl. Mech. Eng. 348 (2019) 334–355.
[19] A. Tasora, R. Serban, H. Mazhar, A. Pazouki, D. Melanz, J. Fleischmann, M. Taylor, H. Sugiyama, D. Negrut, Chrono: an open source multi-physics dynamics engine, in: T. Kozubek (Ed.), High Performance Computing in Science and Engineering–Lecture Notes in Computer Science, Springer 2016, pp. 19–49.
[20] The CGAL Project, CGAL User and Reference Manual, 4.11 edition CGAL Editorial Board, 2017.
[21] S.A. Silling, M. Epton, O. Weckner, J. Xu, A. Askari, Peridynamics states and constitutive modeling, J. Elast. 88 (2) (2007) 151–184.
[22] E. Madenci, E. Oterkus, Peridynamic Theory and Its Applications, Springer, New York, 2014.
[23] F. Zhu, J. Zhao, A peridynamic investigation on crushing of sand particles, Géotechnique 69 (6) (2019) 526–540.
[24] M. Jean, The non-smooth contact dynamics method, Comput. Methods Appl. Mech. Eng. 177 (3–4) (1999) 235–257.
[25] M. Servin, D. Wang, C. Lacoursière, K. Bodin, Examining the smooth and nonsmooth discrete element approaches to granular matter, Int. J. Numer. Methods Eng. 97 (12) (2014) 878–902.
[26] M. Anitescu, A. Tasora, An iterative approach for cone complementarity problems for nonsmooth dynamics, Comput. Optim. Appl. 47 (2) (2010) 207–235.
[27] A. Tasora, M. Anitescu, A convex complementarity approach for simulating large granular flows, J. Comput. Nonlinear Dyn. 5 (3) (2010), 031004.
[28] T.D. Heyn, On the Modeling, Simulation, and Visualization of Many-body Dynamics Problems With Friction and Contact, PhD Dissertation University of Wisconsin-Madison, 2013.
[29] D. Negrut, R. Serban, A. Tasora, Posing multibody dynamics with friction and contact as a differential complementarity problem, J. Comput. Nonlinear Dyn. 13 (1) (2018), 014503.
[30] M. Kwarta, D. Negrut, Using the complementarity and penalty methods for solving frictional contact problems in Chrono: validation for the cone penetration test, Technical Report TR-2016-16, Simulation-Based Engineering Lab, University of Wisconsin-Madison, 2017.
[31] A.R. Russell, D.M. Wood, Point load tests and strength measurements for brittle spheres, Int. J. Rock Mech. Min. Sci. 46 (2009) 272–280.
[32] H.J. Ryu, F. Saito, Single particle crushing of nonmetallic inorganic brittle materials, Solid State Ionics 47 (1991) 35–50.
[33] S. Luding, E. Clement, A. Blumen, J. Rajchenbach, J. Duran, Studies of columns of beads under external vibrations, Phys. Rev. E 49 (2) (1994) 1634–1646.
[34] F. da Cruz, S. Emam, M. Prochnow, J.N. Roux, F. Chevoir, Rheophysics of dense granular materials: discrete simulation of plane shear flows, Phys. Rev. E 72 (2) (2005), 021309.
[35] P.J. Barrett, The shape of rock particles, a critical review, Sedimentology 27 (3) (1980) 291–303.
[36] H. Wadell, Volume, shape, and roundness of rock particles, J. Geol. 40 (1932) 443–451.
[37] W.C. Krumbein, Measurement and geological significance of shape and roundness of sedimentary particles, J. Sediment. Petrol. 11 (1941) 64–72.
[38] S.J. Blott, K. Pye, Particle shape: a review and new methods of characterization and classification, Sedimentology 55 (1) (2008) 31–63.
[39] G. Mollon, J. Zhao, Fourier-Voronoi-based generation of realistic samples for discrete modeling of granular materials, Granul. Matter 14 (2012) 621–638.
[40] G. Mollon, J. Zhao, 3D generation of realistic granular samples based on random fields theory and Fourier shape descriptors, Comput. Methods Appl. Mech. Eng. 279 (2014) 46–65.
[41] R. Rorato, M. Arroyo, E. Ando, A. Gens, Sphericity measures of sand grains, Eng. Geol. 254 (2019) 43–53.
[42] G.R. McDowell, A. Amon, The application of Weibull statistics to the fracture of soil particles, Soils Found. 40 (5) (2000) 133–141.
[43] Y. Nakata, A.F.L. Hyde, M. Hyodo, H. Murata, A probabilistic approach to sand particle crushing in the triaxial test, Géotechnique 49 (5) (1999) 567–583.
[44] H.Y. Li, H.W. Chai, X.H. Xiao, J.Y. Huang, S.N. Luo, Fractal breakage of porous carbonate sand particles: microstructures and mechanisms, Powder Technol. 363 (2020) 112–121.
[45] G.R. McDowell, On the yielding and plastic compression of sand, Soils Found. 42 (1) (2002) 139–145.
[46] N.P. Daphalapurkar, F. Wang, B. Fu, H. Lu, R. Komanduri, Determination of mechanical properties of sand grains by nanoindentation, Exp. Mech. 51 (2011) 719–728.
[47] M. Otsubo, C. O'Sullivan, K.J. Hanley, W.W. Sim, The influence of particle surface roughness on elastic stiffness and dynamic response, Géotechnique 67 (5) (2017) 452–459.
[48] R.A. Zeleny, E.L. Piret, Dissipation of energy in single particle crushing, Ind. Eng. Chem. Process Des. Dev. 1 (1) (1962) 37–41.
[49] K. Kendall, The impossibility of comminuting small particles by compression, Nature 272 (1978) 710–711.
[50] F.N. Altuhafi, M.R. Coop, The effect of mode of loading on particle-scale damage, Soils Found. 51 (5) (2011) 849–856.
[51] Q. Liu, W. Xiang, M. Budhu, D. Cui, Study of particle shape quantification and effect on mechanical property of sand (in Chinese), Rock Soil Mech. 32 (Suppl. 1) (2011) 190–197.
[52] T. Ueda, T. Matsushima, Y. Yamada, DEM simulation on the one-dimensional compression behavior of various shaped crushable granular materials, Granul. Matter 13 (5) (2013) 675–684.
[53] G. Ma, Y. Chen, F. Yao, W. Zhou, Q. Wang, Evolution of particle size and shape towards a steady state: insights from FDEM simulations of crushable granular materials, Comput. Geotech. 112 (2019) 147–158.
[54] G.R. McDowell, M.D. Bolton, D. Robertson, The fractal crushing of granular materials, J. Mech. Phys. Solids 44 (12) (1996) 2079–2101.
[55] J.C. Jaeger, Failure of rocks under tensile conditions, Int. J. Rock Mech. Min. Sci. 4 (2) (1967) 219–227.
[56] I. Einav, Breakage mechanics – part I: theory, J. Mech. Phys. Solids 55 (6) (2007) 1274–1297.
[57] Y. Zhang, G. Buscarnera, Breakage mechanics for granular materials in surface-reactive environments, J. Mech. Phys. Solids 112 (2018) 89–108.
[58] F. Zhu, J. Zhao, Multiscale modeling of continuous crushing of granular media: the role of grain microstructure, Comput. Part. Mech. (2020) https://doi.org/10.1007/s40571-020-00355-0.